Acoustic Tag Identification Based on Noncoherent FSK Detection With Portable Devices

Fernando J. Álvarez, *Senior Member, IEEE*, Teodoro Aguilera, José A. Paredes, and José A. Moreno

***Abstract*— This paper presents a tag identification system based on the detection of high-frequency acoustic signals by means of a portable device. A binary frequency shift keying-modulated code is used to tag the different locations. This code is preceded by a synchronizing chirp waveform that allows noncoherent detection even under strong Doppler frequency shifts. The proposed system is first characterized in terms of robustness against noise, coverage, Doppler tolerance, and intertag interference, making use of a modular simulator. This simulator is based on three basic stages that account for the frequency response of the emitter–receiver pair, the attenuation of acoustic signals in air, and the noncoherent demodulation. This system is then implemented in an Android-based platform and tested in a real scenario. The results of this experimental analysis show good agreement with the previous characterization, and they also confirm the feasibility of the proposed system to develop location-aware applications.**

***Index Terms*— Acoustic tag identification, android-based platform, noncoherent FSK detection, portable device.**

I. Introduction

CONTEXT awareness is gaining increasing applicability in interactive mobile computing systems, which can provide users with a customized experience based on their contextual information [1]. An essential part of this information is the user location, supported by Global Navigation Satellite Systems (GNSSs) in outdoor environments. Unfortunately, due to multipath propagation and the attenuation effect caused by walls and roofs, the GNSS has very low accuracy or cannot fix a position at all in indoor environments, where much human activity takes place [2]. To extend location availability to these environments, new technological possibilities, such as Wi-Fi [3], [4], ultrawideband (UWB) [5], [6], magnetic [7]–[9], or acoustic [10]–[12] have been proposed and are still a subject of intense research.

Manuscript received December 7, 2016; revised September 14, 2017; accepted October 31, 2017. Date of publication December 12, 2017; date of current version January 4, 2018. This work was supported in part by the European Commission through the Project LIMUS under Grant 0246-LIMUS-4-E, in part by the Spanish Government and the European Regional Development Fund (ERDF) through the Project TARSIUS under Grant TIN2015-71564-C4-4-R, and in part by the Regional Government of Extremadura and ERDF-ESF under Project GR15167 and through the Pre-Doctoral Scholarship under Grant 45/2016 Exp. PD16030. The Associate Editor coordinating the review process was Dr. Shervin Shirmohammadi. *(Corresponding author: Fernando J. Álvarez.)*

The authors are with the Department of Electrical Engineering, Electronics and Automation, University of Extremadura, E-06006 Badajoz, Spain (e-mail: fafranco@unex.es; teoaguibe@unex.es; japaredesm@unex.es; josan@unex.es).

Color versions of one or more of the figures in this paper are available online at http://ieeexplore.ieee.org.

Digital Object Identifier 10.1109/TIM.2017.2777578

Nevertheless, many context-aware applications do not require an exact position of the user in a common coordinate system but rather the identification of close-by and tagged points of interest. Most tag identification systems are based on radio frequency identification (RFID), where tags and readers exchange information via electromagnetic fields and under a specific communication protocol [13]–[19]. Some of these works propose an indoor tracking system for mobile objects equipped with an RFID tag [20] or even combine RFID with the UWB to increase the tag identification efficiency [21]. The main drawback of this technology is the possibility of collision between emissions from several tags, both in a single reader [22] and a multireader system [23]. Besides, most current smartphones and tablets are not equipped with RFID sensors. The near-field communication technology, which is based on RFID principles [24], solves the collision problem but has a sensing range of less than 10 cm that limits the possibilities of a practical interaction. Barcode or QR-tag scanning is an inexpensive possibility, but again it requires a close interaction from the user, who has to focus the device camera onto the code [25].

The Bluetooth technology has also been used for the purpose of tag identification. It improves RFID in terms of power consumption [26]–[28], but unfortunately it does not solve the interference problem between different tags and also with Wi-Fi networks with which it shares the frequency band [29]. Bluetooth receivers are integrated in most portable devices today, but the access to this receiver is often limited by the operating system.

An interesting alternative is provided by the acoustic technology. Nowadays, there is a renewed interest in the design of acoustic systems for accurate location of portable devices. One of the main disadvantages that traditionally attributed to acoustic systems is their limited coverage, due to both the narrow beamwidth and short propagation range of high-frequency acoustic signals. Nevertheless, this in principle unfavorable feature could be exploited to conduct a precise short-range cell identification of great interest for some applications. Some works have already proposed this solution to develop museum smartguides that work in the low-frequency ultrasonic range [30] or the high-frequency audible range [31]. However, these works provide very scarce technical details, since they focus their results on the analysis of the visitors satisfaction. None of these works provide enough information to replicate the proposed system, nor do they conduct a rigorous study of detection hindering phenomena, such as the presence of noise, intertag interference, or the effect of the user movement.

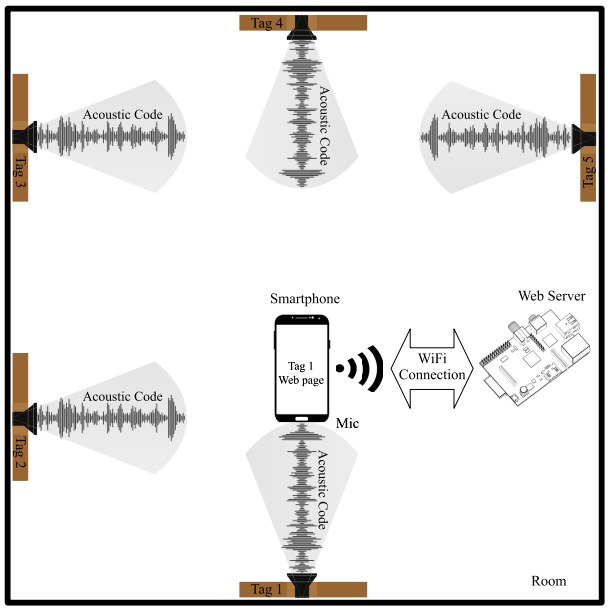

Fig. 1. Application example of the proposed tag identification system.

In this paper, we present a complete description of all the elements that compose an acoustic tag identification system, based on the noncoherent FSK detection of high-frequency audible signals with a portable device. A software model based on three basic stages is developed and next used to characterize the system in terms of robustness against noise, coverage, Doppler tolerance, and intertag interference. This system is then implemented in an Android-based platform and experimentally tested in a real scenario.

The rest of this paper is organized as follows. Section II describes the main features of the proposed system, including the global architecture, the acoustic tags, and the portable receiver. In Section III, the system is modeled and characterized by simulation. Section IV presents the implementation details and some experimental results obtained in a real scenario. In Section V, the main limitations of the proposed system are discussed and some lines of improvement are outlined. Finally, the main conclusions of this paper are summarized in Section VI.

II. System Overview

A. Global Architecture

The global architecture of the proposed system can be described with the help of the application example shown in Fig. 1. A set of independent acoustic tags are deployed in a room or building each covering a reduced area in front of them. When the receiver, a portable device, is in one of these areas with its microphone pointing toward the tag, it receives an encoded emission that identifies the tag unambiguously. Making use of a Wi-Fi connection, this code is sent to a local server based on a Raspberry Pi 3B platform [32] that provides the receiver with contextual information. This information can be just the tag location and some navigation instructions; in such case, the system behaves as an area identification-based positioning system, where the user is assigned the location of the beacon that provides coverage [33]. Needless to say, richer information related to the tag emplacement could be provided to the user, as for example, a detailed multimedia description of a certain artwork in a museum room [34].

Fig. 2. Picture of the Kingstate KSSG1708 transducer.

B. Acoustic Tags

To tag the different locations, we have used a Kingstate KSSG1708 high-frequency transducer [35] that presents a maximum frequency response at 20 kHz, with a sound pressure level of 87 dB at 10 cm (see Fig. 2).

This transducer is driven by a class-D audio amplifier and a low-cost STM32L476VG microcontroller [36], which stores a binary frequency shift keying (BFSK)-modulated code that uniquely identifies it. Fig. 3(a) shows the block diagram of the acoustic tag. The length of this code is N bits, where N is the first integer above $\log_2 M$, and M is the number of locations to be tagged. These bits are BFSK-modulated using the frequencies of $f_0 = 17$ kHz and $f_1 = 19$ kHz for bits 0 and 1 respectively, with 15 carrier cycles per modulation symbol, thus giving an average message duration

$$T_m \approx \frac{15 \cdot N}{2}\left(\frac{1}{f_0}+\frac{1}{f_1}\right) \approx N \times 836\,\mu s. \tag{1}$$

This message is preceded by a chirp header used to signal the beginning of the message through matched filtering. The chirp waveform sweeps over the frequency range of 16–20 kHz in a time interval of $T_c = 4$ ms, thus featuring a time-bandwidth product of 16 that ensures good autocorrelation properties for this purpose. This waveform has been chosen over other signals with similar deltalike autocorrelation function (such as pseudorandom sequences) due to its better tolerance to Doppler frequency shifts [37]. After the emission, the transducer is silent for a time T_s, thus giving a total emission period

$$T_e = T_c + T_m + T_s. \tag{2}$$

C. Portable Receiver

As stated before, the proposed system is based on the user's portable device. This device is programmed to demodulate the above-described signal by following the noncoherent FSK detection scheme shown in Fig. 3. As shown in Fig. 3, the received signal is first digitized at a sampling rate of $f_s = 96$ kHz and then matched filtered to synchronize the beginning of the binary message through the chirp autocorrelation peak. This message is then bandpass-filtered with two parallel digital filters centered at the FSK carrier frequencies with a 2-kHz bandwidth. These equiripple finite-impulse response (FIR) filters feature a linear phase response and have

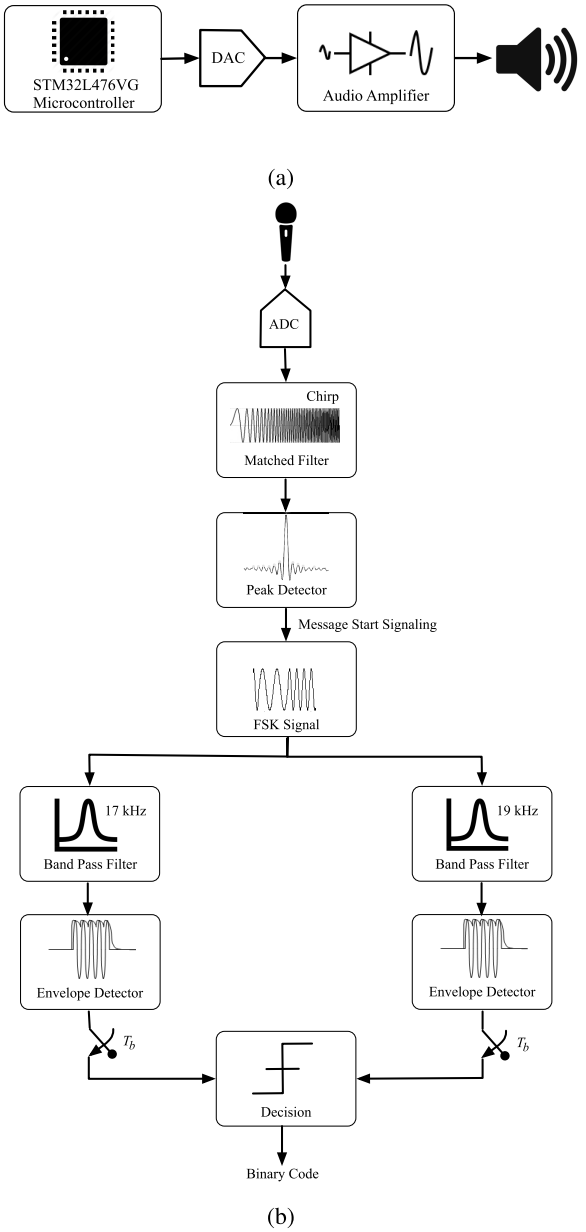

Fig. 3. Block diagram of (a) acoustic tag and (b) proposed receiver (noncoherent FSK detector).

been designed to present a maximum ripple of 1 dB in the passband and a minimum attenuation of 55 dB in the stopband. The envelope of these filters' output is then obtained and sampled at the bit rate (T_b) to feed the decision stage that ultimately provides the binary code.

III. System Characterization

After the general overview provided previously, this section aims to characterize the acoustic tag identification system in terms of robustness against noise, coverage, Doppler tolerance, and intertag interference. This characterization is performed by means of a modular simulator based on three basic stages, which have been entirely programmed from scratch in MATLAB. The first of these stages models the frequency

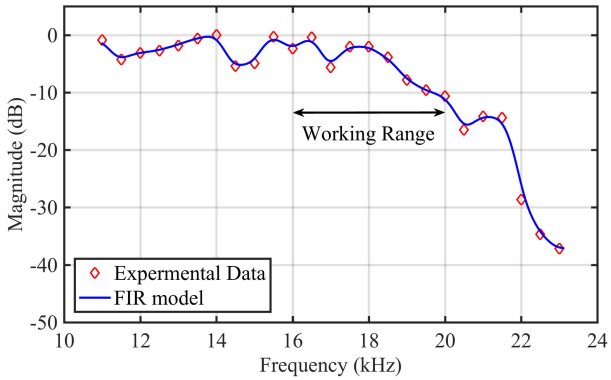

Fig. 4. Frequency response of the emitter–receiver pair.

response of the emitter–receiver pair that has been experimentally obtained in our laboratory by placing the mobile device at a distance of 1 m from the Kingstate KSSG1708 transducer over its acoustic axis. Fig. 4 shows both the experimental response (red diamonds) and that of the FIR filter designed to model this behavior (blue line). Fig. 4 also shows the frequency working range from 16 to 20 kHz, which has been selected with a threefold objective: 1) work in a low loudness zone of the human ear; 2) generate short duration emissions; and 3) restrict the angular and range coverage of the acoustic tag.

The second stage of our simulator accounts for the attenuation of acoustic waves in the air, and it considers atmospheric absorption as predicted by the ISO 9613 norm [38] and geometrical spreading. Hence, the acoustic pressure at a distance of r meters from the emitter is obtained by this stage as

$$P(r)\ (\text{dB}) = P_0 - 20\log r - 8.68 \cdot \alpha(f)(r - r_0) \qquad (3)$$

where P_0 is the acoustic pressure at the reference distance of $r_0 = 1$ m, and $\alpha(f)$ is the frequency-dependent absorption coefficient given by the ISO norm.

Finally, the last stage in our model simulates the behavior of the noncoherent FSK detector already described in Section II-C, assuming the transmission of $N = 8$-bit codes and a silent time of 20 ms, for a total emission period of $T_e = 4 + 8 \times 0.836 + 20 = 30.688$ ms.

A. Robustness Against Noise

To analyze the performance of the proposed system in noisy conditions, different levels of SNR ranging from 0 to 15 dB in increments of 3 dB have been considered at the reference distance of $r_0 = 1$ m. For each SNR level, a total of 25 600 emissions (100 emission $\times$ 256 codes) have been simulated at different ranges, from 1 to 4 m in increments of 10 cm. The total number of successful detections thus obtained is represented in Fig. 5. As can be seen, the presence of noise has a noticeable effect on the system performance, and success rates below 90% are obtained at the reference distance of 1 m with SNR levels below 6 dB. Nevertheless, with an SNR of 15 dB at 1 m, a 100% success rate is obtained at this reference distance, and values above 60% are obtained at ranges as far as 4 m.

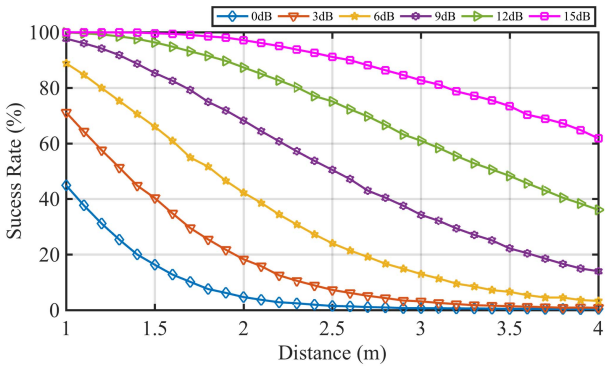

Fig. 5. Detection success rate with range at different SNR levels.

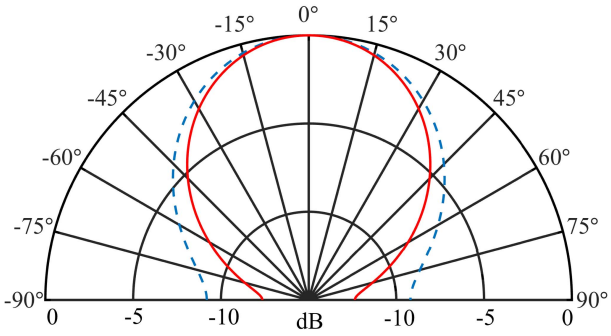

Fig. 6. Piston-shaped transducer directivity patterns at 17 kHz (blue dashed line) and 19 kHz (red solid line).

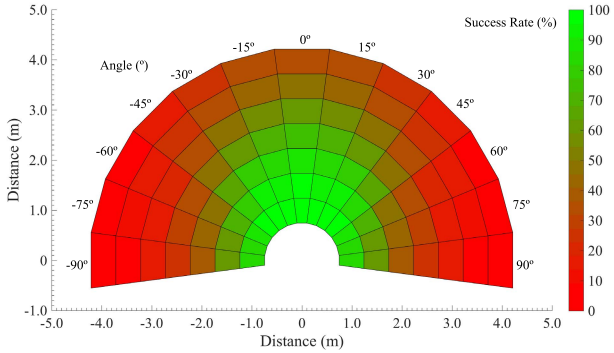

Fig. 7. Detection success rate with range and bearing angle.

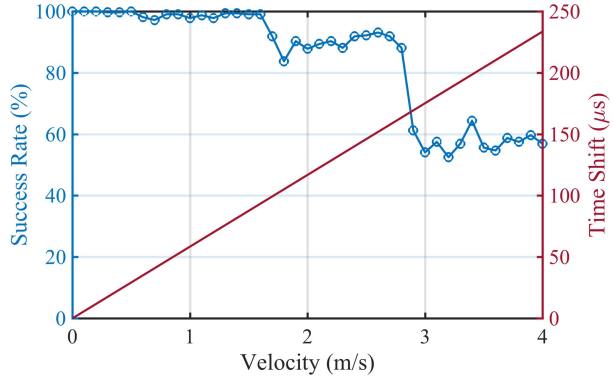

Fig. 8. Detection success rate (blue solid line) and shift of the chirp autocorrelation peak (red dashed line) with receiver speed.

B. Coverage

To study the system coverage, a new stage has been added to our model that simulates the filtering effect associated with the transducer emission pattern. For a piston-shaped transducer as the Kingstate KSSG1708 represented in Fig. 2, this pattern can be expressed as [39]

$$D(\varphi,\theta) = D(\theta) = \frac{2J_1(k \cdot a \sin\theta)}{k \cdot a \sin\theta} \tag{4}$$

where a is the radius of the piston, $k = 2\pi/\lambda$ is the wavenumber, θ is the angle respect to the acoustic axis, and J_1 is the first-order Bessel function of the first kind. Fig. 6 shows this pattern for the Kingston transducer ($a = 8.5$ mm) and the two carrier frequencies $f_0 = 17$ kHz and $f_1 = 19$ kHz. Note that, for a fixed angle θ, (4) gives the response of the transducer as a function of the wavenumber k, or equivalently, it represents the frequency response of the transducer in a given direction. It is easy to see from this expression that, for any angle different from $\theta = 0°$ (propagation along the acoustic axis), D is a function of k and the transducer behaves as a filter of the emitted signal.

In this paper, 91 test positions have been defined around the transducer, at ranges from 1 to 4 m in increments of 0.5 m and bearing angles from $-90°$ to $90°$ in increments of 15°. In each one of these positions, 25 600 emissions have been again simulated assuming an SNR of 12 dB at 1 m over the acoustic axis. Fig. 7 shows the rate of successful detections at different ranges and bearing angles, where the consequences of the filtering effect predicted by (4) can be appreciated.

C. Doppler Tolerance

One of the most important features of the proposed system is the Doppler-shift tolerance inherited from both the header chirp and the noncoherent FSK detection. This phenomenon can be simulated with a new stage that assumes a virtual sampling frequency at the receiver f_s' given by

$$f_s' = f_s \cdot \left(1 + \frac{v_r}{c}\right) \tag{5}$$

where f_s is the actual sampling frequency (96 kHz), v_r is the radial speed of the receiver with respect to the emitter (positive if approaching), and c is the speed of sound in air. From these virtual samples, the signal acquired at the actual sampling rate is then obtained by cubic interpolation.

In this paper, different radial velocities from 0 to 4 m/s have been assumed for a receiver placed at the reference distance of $r_0 = 1$ m, with an SNR value of 12 dB. Fig. 8 shows the detection success rate for different radial speeds of the receiver. As can be seen in Fig. 8, rates around 90% are obtained for receiver speeds up to 2.8 m/s, which are very unlikely to be surpassed in typical applications of this system. Note that this upper limit is much lower than the one imposed by the filtering of the frequency-shifted carriers, which is roughly given by

$$v_{r,\max} \approx \frac{\mathrm{BW} \cdot c}{2 f_c} \tag{6}$$

where f_c is the carrier frequency and BW is the bandwidth of the receiver's bandpass filters. For BW = 2 kHz, this limit

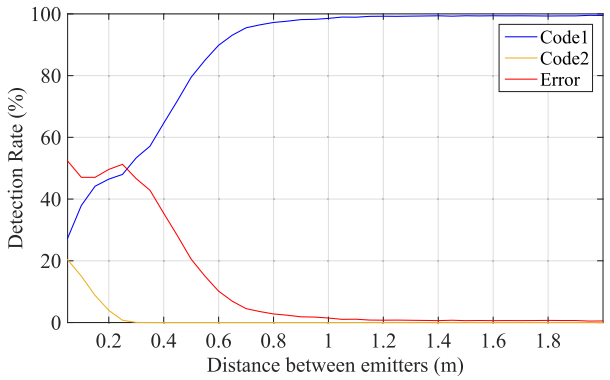

Fig. 9. Code detection rates under intertag interference.

will be $v_{r,\max} \approx 18$ m/s. The Doppler shift resilience of this system is actually determined by the time shifting of the chirp autocorrelation peak used to synchronize the beginning of the message, which is given by [37]

$$\tau_{\text{shift}} = \Delta f \cdot \frac{T}{B} \tag{7}$$

where $\Delta f = f \cdot v_r/c$ is the central frequency shift, T represents the chirp duration, and B represents its frequency expansion. In our case, this expression yields $\tau_{\text{shift}}\ (\mu\text{s}) = 58.3 \cdot v_r$.

This time shift has been represented in Fig. 8 together with the detection success rate. As can be seen, a significant decrease of this rate occurs at $v_r = 2.9$ m/s, when the time shift reaches around 20% of the bit duration (169 μs).

D. Intertag Interference

Finally, the interference between different tags has been investigated by assuming the presence of a second tag emitting a different code in the same vertical plane (wall) than the first one, placed at the same height but at a variable distance of d meter from it. As before, the receiver is located at a reference range of $r_0 = 1$ m over the acoustic axis of tag 1, and thus at a range of $(1 + d^2)^{1/2}$ from tag 2. This new analysis must consider the filtering effect that the microphone's reception pattern has on the signal coming from tag 2. Since the manufacturer of the portable device does not provide any information regarding this pattern, we have experimentally tested it at the carrier frequencies to obtain a high directionality model with 3 dB loss at 15° and 9 dB loss at 30°.

Fig. 9 shows the detection rate of codes 1 and 2 for distances of separation between the corresponding tags ranging from 5 to 200 cm in increments of 5 cm. For each distance, 10 000 emissions have been simulated, assuming a random delay between codes 1 and 2 at the receiver with a uniform distribution between a minimum value of $-T_s/2 = -10$ ms and a maximum of $T_s/2 = 10$ ms. This random delay accounts for the complete absence of synchronism between different tags in the real system. As can be seen in Fig. 9, detection rates above 90% are obtained for code 1 when the interfering tag 2 is further than 60 cm. Below this limit, the detection rate of code 1 decreases to a value of 30% at the minimum separation distance of 5 cm. Also, note that as the separation distance decreases below 30 cm, there is an increasing nonzero probability of detecting code 2, although this probability is always below the probability of detecting an erroneous code.

Finally, it is important to remark that this analysis is independent of the codes emitted by the acoustics tags, since almost identical results to those represented in Fig. 9 have been obtained when choosing different pairs of codes.

IV. Implementation and Experimental Results

The practical implementation of the receiver described in Section II-C has been performed on an LG X Screen (LGK500N [40]) mobile phone, equipped with 2 GB of RAM memory and a Quad-Core Qualcomm Snapdragon 410 MSM8916v2 processor at 1.4 GHz. This phone incorporates the Android 6.0 Marshmallow operating system that allows the required 96-kHz sampling frequency. All signal processing is carried out off-line, by first acquiring a number of samples high enough as to ensure the acquisition of two consecutive emissions $(2 \cdot T_e - T_s)$. This size guarantees that the emitted signal will be captured entirely inside the buffer at least once. After being acquired, the signal is processed in the frequency domain using the fast Fourier transform supplied by the JTransforms libraries [41]. These libraries are used due to their good performance in correlation and convolution tasks. All the programming has been conducted making use of the Android Studio Software Development Kit [42].

Fig. 10(a) shows an example of the actual signal acquired by the smartphone when placed at one meter distance from the tag emitting the test code $c1 = \{10101010\}$. Fig. 10(b) shows this signal after correlation with the chirp waveform and Fig. 10(c) shows the outputs of the 17 and 19 kHz centered bandpass filters with red and blue regions, respectively. As explained before, these signals' envelopes are sampled at the bit rate and fed to the decision stage that ultimately determines the bit transmitted.

The coverage of the acoustic tag has also been experimentally analyzed by placing the smartphone in the same 91 test positions defined in Section III-B. In each one of these positions, 100 emissions of the test code $c1$ have been performed to compute the detection success rate represented in Fig. 11. An actual SNR of 12 dB was measured at 1 m from the emitter during this experimentation. As can be seen, these results are in good agreement with the simulated ones represented in Fig. 7, although some differences can be observed between Figs. 7 and 11. The tag actual coverage seems to be larger than the simulated one both in range and bearing angle, and it also presents some discontinuities that cannot be observed in Fig. 7. These differences can be partially explained by the presence of multipath in the real system, as a consequence of the floor reflections that have not been simulated in the model. Also, the noise measured in the real scenario is unlikely to be the white Gaussian noise considered in the simulation, and its effect on the detection process could be less harmful than predicted.

To experimentally study the Doppler tolerance of the system, an electric slider has been mounted in front of an acoustic tag with an attached platform where the smartphone has been placed (see Fig. 12). This slider is a 2-m long conveyor belt,

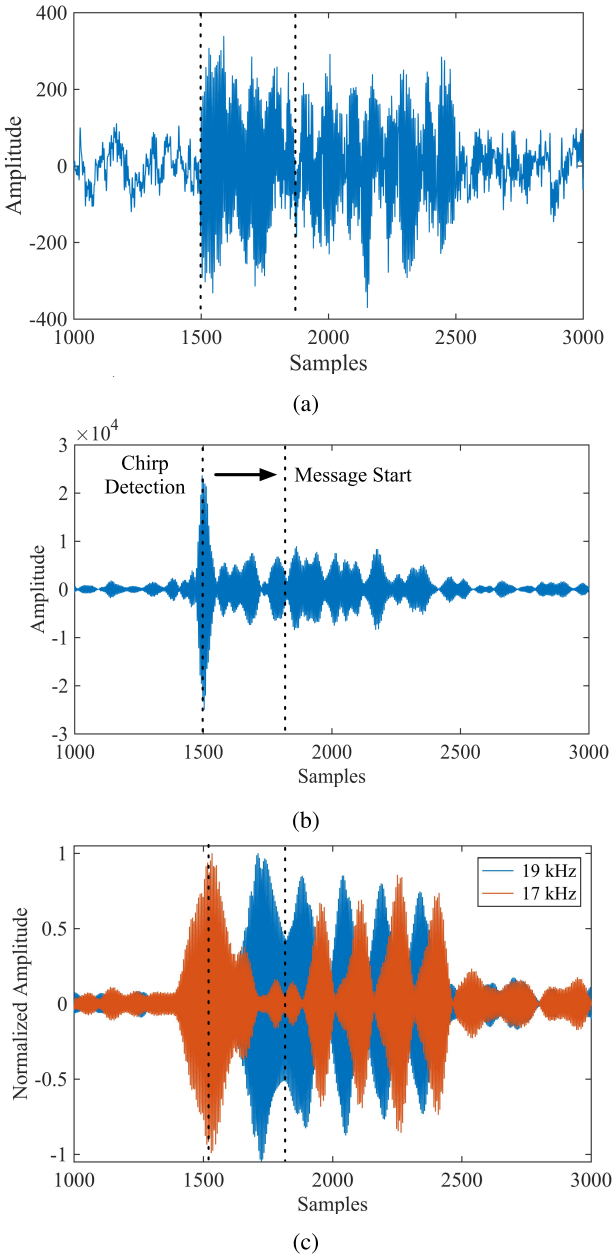

Fig. 10. (a) Actual signal acquired by the smartphone, (b) output of the matched filter showing the chirp autocorrelation peak that signals the message start, and (c) outputs of the 17 kHz (red region) and 19 kHz (blue region) centered bandpass filters used to detect the zeros and ones, respectively.

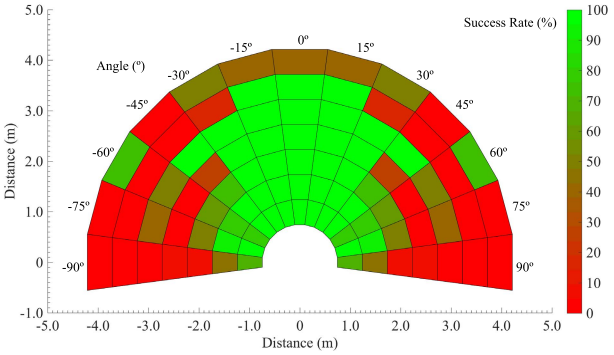

Fig. 11. Experimental detection success rate with range and bearing angle.

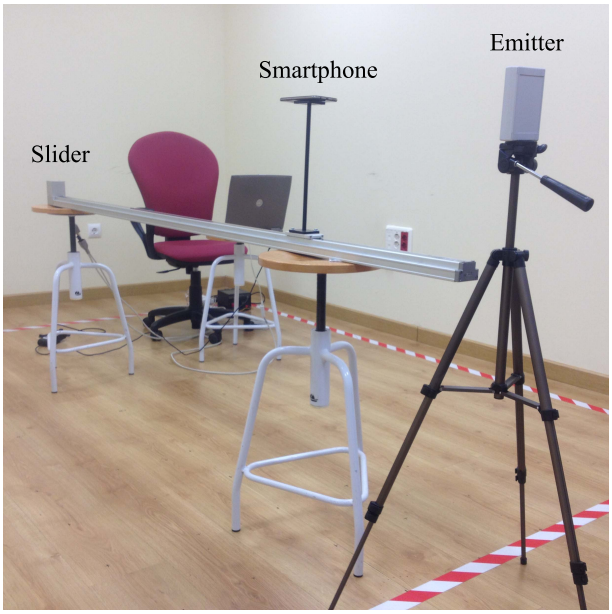

Fig. 12. Experimental setup to analyze the Doppler shift tolerance.

which is capable to reach a maximum speed of 2 m/s with maximum acceleration values of ± 3 m/s^2, thus providing a maximum analysis window of 333 ms at this speed.

Fig. 13(a) shows the actual signal acquired by the smartphone during an approaching trajectory with a 330-ms constant speed window centered around the $r_0 = 1$ m reference distance from the tag. As can be seen, this signal is polluted with the strong noise produced by the displacement of the slider. Fig. 13(b) shows this signal after correlation with the chirp, where the different emissions can be clearly distinguished despite the intense noise. Fig. 13 also shows the constant speed window where all the emissions were received by the smartphone approaching at 2 m/s. This test has been repeated ten times, and all the receptions in the constant speed window has been processed to obtain a detection success rate of 75% that is significantly lower than the value predicted in Section III-C. Although it could be argued that the cause of this decrease must be the intense noise produced by the slider, a more in the depth analysis of these data has revealed that the energy of this noise in mostly in the low-frequency range with very limited impact on the system performance. The main cause of the reduced performance may have a double source. First source is the interference caused by the specular reflections of the emitted signals on the slider that affect a small amount of the signals acquired in the constant speed window. Second source is the interactions between the different sound sources due to the nonlinear parametric effects [43].

Intertag interference has been experimentally studied by using a second tag to emit the code $c2 = \{01010101\}$. This tag has been placed in the test positions defined in Section III-D. In each one of these positions, 100 emissions of codes $c1$ and $c2$ have been performed to obtain the detection rates shown in Fig. 14. Once again, the real results exhibit a better behavior than the simulated ones presented in Fig. 9.

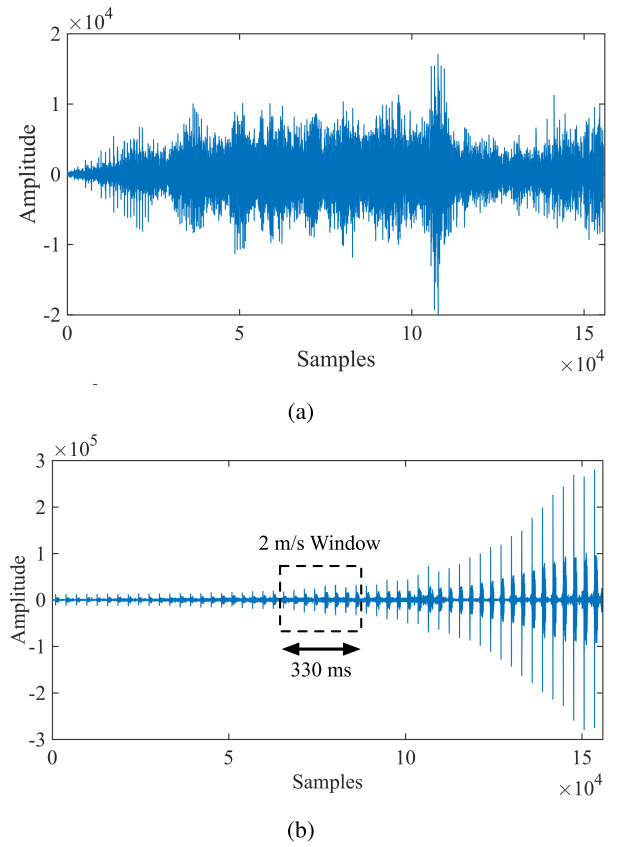

Fig. 13. (a) Actual signal received during the Doppler shift trial and (b) this signal after correlating with the header chirp.

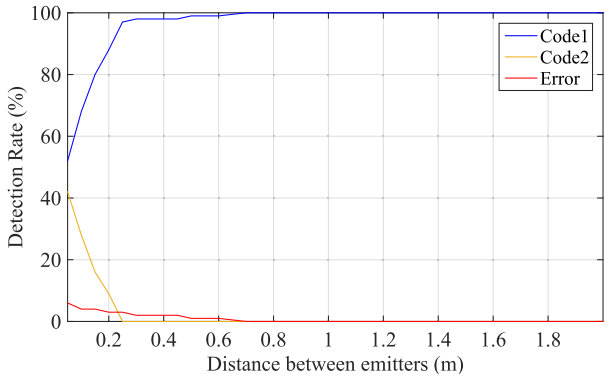

Fig. 14. Experimental code detection rates under intertag interference.

Now, detection rates above 90% are obtained for code 1 when the tags are separated by distances above 20 cm. Below this distance, as predicted by simulation, the detection rate of code 1 decreases to reach a minimum at the separation distance of 5 cm. As can be observed, besides this better behavior of the success rate, the main difference between the simulated and the real results is that in the latter ones, the detection rate of code 2 is higher than the detection rate of an erroneous code for distances below 30 cm. This result could be a consequence of the delay between codes 1 and 2 taking a particular set of values during the experimental testing, since this delay was considered a uniformly distributed random variable in the simulation.

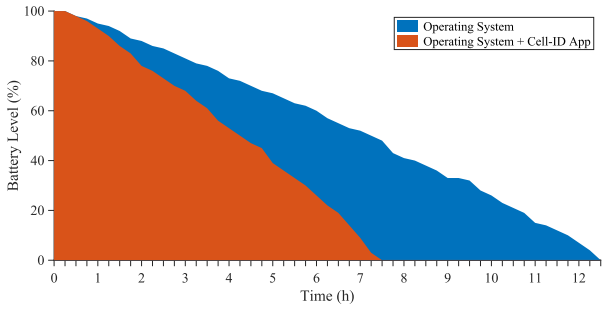

Fig. 15. Battery power consumption.

Finally, it has been considered interesting to analyze the battery consumption of the developed tag identification application. Fig. 15 compares the battery discharge rate of the LG X Screen smartphone when running just the operative system with Wi-Fi connectivity and when running our application continuously. As can be seen, the application reduces a 40% the discharge period, but this period is still above 7 h. Also, note that during a typical use of this application, it will be only activated occasionally, notably reducing the battery consumption in practice.

V. Discussion

The tag identification system described in Sections II and III can easily be deployed in a building at a very reduced cost, and it is also easily scalable, since the number of tagged locations can be increased by simply enlarging the length of the FSK message. Users can identify these tags just by installing an application in their portable devices, without the need of any additional hardware. It is important to remark that although this application has been implemented in an Android-based platform, its extension to other mobile platforms, such as iOS or Windows Phone, would be straightforward as far as they provide high enough sampling rates. Also, note that since this system operates in the high-frequency audible range (16–20 kHz), it is immune to most acoustic sources that can be usually found indoors, including human talking.

There are, however, some important design aspects that must be discussed to clearly state the system limitations and to define future lines of improvement. One of the most important shortcomings of the proposed system is the sonority of the emitted signals, which are imperceptible for most adults but can be heard by teenagers and children. The power transmitted by a single tag is small, causing the sound pressure level to increase from 40 dB (room noise level) to 52 dB at 1 m from the tag. Nevertheless, this effect could become bothersome with a high density of tags in the same room. Note that the need to work in the audible range is imposed by the frequency response of the portable device microphone that falls off rapidly beyond 20 kHz in most commercial devices. However, some manufacturers are starting to realize the possible applications of incorporating ultrasonic microphones in their devices, a trend that would solve this problem. In the meantime, further signal processing could be applied to reduce the emissions sonority at the expense of slightly worsening the detection performance and increasing the computation time.

A second aspect which is worth some attention is the tag's power consumption. In this paper, the tags have been designed to emit a new message approximately every 30 ms, thus allowing a fast detection of this message by the listening receiver. This configuration is not a problem if the tags are connected to the power network, but could be unfeasible for battery-powered tags. This problem could be tackled by designing reactive tags that would only provide a new emission every time they are requested to do so by the user. This approach would also mitigate the sonority problem described in the previous paragraph.

Finally, although this tag identification system has been designed to operate indoors, it would be very interesting to analyze its performance in open spaces where it would find direct application, such as parks, open plazas, or parking lots. These are very challenging environments for the propagation of acoustic waves due to the wide variations of temperature and humidity, the presence of wind gradients, and the generation of turbulent vortices. A detailed analysis of the effects of all these phenomena on the performance of the system should be conducted prior to exporting it to outdoor spaces.

VI. Conclusion

This paper has presented a tag identification system based on the detection of high-frequency acoustic signals with a portable device. This system is based on a set of independent tags that emit a BFSK-modulated code to identify them unambiguously. Once detected, this code is sent by the portable device to a local server based on a Raspberry Pi 3B platform that provides it with contextual information. Binary codes are detected by performing a noncoherent demodulation, which is synchronized by the matched filtering detection of a chirp header. This demodulation scheme renders the system resilient to the Doppler shift caused by the user movement.

A modular simulator based on three basic stages has been programmed to characterize the system in terms of robustness against noise, coverage, Doppler tolerance, and intertag interference. These stages model the emitter–receiver frequency response, the attenuation of sound in air, and the abovementioned noncoherent demodulation of the BFSK message.

The noncoherent demodulator has been implemented in an Android-based platform that performs all the filtering operations in the frequency domain. The acoustic tags have been designed by driving a Kingstate KSSG1708 high-frequency transducer with a class-D audio amplifier and a low-cost STM32L476VG microcontroller. This system has been tested in an actual scenario to analyze its coverage, Doppler tolerance, and intertag interference. The experimental results show in general good agreement with the previous characterization, although some differences have been observed in favor of the actual system.

Finally, the main limitations of the proposed system have been discussed to clearly state the possible lines of future improvement.

References

[1] G. W. Musumba and H. O. Nyongesa, "Context awareness in mobile computing: A review," *Int. J. Mach. Learn. Appl.*, vol. 2, no. 1, pp. 1–10, 2013.

[2] P. A. Zandbergen, "Accuracy of iPhone locations: A comparison of assisted GPS, WiFi and cellular positioning," *Trans. GIS*, vol. 13, no. s1, pp. 5–25, 2009.

[3] Y. Zhuang, Z. Syed, Y. Li, and N. El-Sheimy, "Evaluation of two WiFi positioning systems based on autonomous crowdsourcing of handheld devices for indoor navigation," *IEEE Trans. Mobile Comput.*, vol. 15, no. 8, pp. 1982–1995, Aug. 2016.

[4] S. He and S.-H. G. Chan, "Wi-Fi fingerprint-based indoor positioning: Recent advances and comparisons," *IEEE Commun. Surveys Tuts.*, vol. 18, no. 1, pp. 466–490, 1st Quart., 2015.

[5] Y. Zhou, C. Law, Y. Guan, and F. Chin, "Indoor elliptical localization based on asynchronous UWB range measurement," *IEEE Trans. Instrum. Meas.*, vol. 60, no. 1, pp. 248–257, Jan. 2011.

[6] W. Suski, S. Banerjee, and A. Hoover, "Using a map of measurement noise to improve UWB indoor position tracking," *IEEE Trans. Instrum. Meas.*, vol. 62, no. 8, pp. 2228–2236, Aug. 2013.

[7] J. Jung, S.-M. Lee, and H. Myung, "Indoor mobile robot localization and mapping based on ambient magnetic fields and aiding radio sources," *IEEE Trans. Instrum. Meas.*, vol. 64, no. 7, pp. 1922–1934, Jul. 2015.

[8] B. Kim and S.-H. Kong, "A novel indoor positioning technique using magnetic fingerprint difference," *IEEE Trans. Instrum. Meas.*, vol. 65, no. 9, pp. 2035–2045, Sep. 2016.

[9] V. Pasku, "A magnetic ranging-aided dead-reckoning positioning system for pedestrian applications," *IEEE Trans. Instrum. Meas.*, vol. 66, no. 5, pp. 953–963, May 2017.

[10] J. C. Prieto *et al.*, "Performance evaluation of 3D-LOCUS advanced acoustic LPS," *IEEE Trans. Instrum. Meas.*, vol. 58, no. 8, pp. 2385–2395, Aug. 2009.

[11] R. Zhang, F. Höflinger, and L. Reindl, "TDOA-based localization using interacting multiple model estimator and ultrasonic transmitter/receiver," *IEEE Trans. Instrum. Meas.*, vol. 62, no. 8, pp. 2205–2214, Aug. 2013.

[12] A. De Angelis *et al.*, "Design and characterization of a portable ultrasonic indoor 3-D positioning system," *IEEE Trans. Instrum. Meas.*, vol. 64, no. 10, pp. 2616–2625, Oct. 2013.

[13] J. Myung, W. Lee, J. Srivastava, and T. K. Shih, "Tag-splitting: Adaptive collision arbitration protocols for RFID tag identification," *IEEE Trans. Parallel Distrib. Syst.*, vol. 18, no. 6, pp. 763–775, Jun. 2007.

[14] Y.-C. Lai and L.-Y. Hsiao, "General binary tree protocol for coping with the capture effect in RFID tag identification," *IEEE Commun. Lett.*, vol. 14, no. 3, pp. 208–210, Mar. 2010.

[15] Z. H. Tee, L. M. Ang, and K. P. Seng, "Smart guide system to assist visually impaired people in an indoor environment," *IETE Tech. Rev.*, vol. 27, no. 6, pp. 455–464, 2010. [Online]. Available: http://www.tandfonline.com/doi/abs/10.4103/02564602.2010.10876779

[16] S. Nainan, R. Parekh, and T. Shah. (Jun. 2013). "RFID technology based attendance management system." [Online]. Available: https://arxiv.org/abs/1306.5381

[17] S. Sen, S. Roy, and S. K. Sarkar, "A proposal for enhancing museum visiting experience implementing active RFID technology," in *Proc. 4th Int. Conf. Adv. Comput. Commun.*, Aug. 2014, pp. 295–298.

[18] F. Sahba, "Museum automation with RFID," in *Proc. World Autom. Congr. (WAC)*, Aug. 2014, pp. 19–22.

[19] A. El-Awamry, M. Khaliel, A. Fawky, and T. Kaiser, "A novel multi-tag identification technique for frequency coded chipless RFID systems based on look-up-table approach," in *Proc. 11th Eur. Conf. Antennas Propag. (EUCAP)*, Mar. 2017, pp. 2070–2074.

[20] S. Seol, E.-K. Lee, and W. Kim, "Indoor mobile object tracking using RFID," *Future Generat. Comput. Syst.*, vol. 76, pp. 443–451, Nov. 2017. [Online]. Available: http://www.sciencedirect.com/science/article/pii/S0167739X16302552

[21] A. Vizziello and P. Savazzi, "Efficient RFID tag identification exploiting hybrid UHF-UWB tags and compressive sensing," *IEEE Sensors J.*, vol. 16, no. 12, pp. 4932–4939, Jun. 2016.

[22] D. Benedetti, G. Maselli, and C. Petrioli, "PrIME: Priority-based tag identification in mobile RFID systems," *Comput. Commun.*, vol. 108, pp. 64–77, Aug. 2017. [Online]. Available: http://www.sciencedirect.com/science/article/pii/S0140366417304668

[23] X. Liu, B. Xiao, F. Zhu, and S. Zhang, "Let's work together: Fast tag identification by interference elimination for multiple RFID readers," in *Proc. IEEE 24th Int. Conf. Netw. Protocols (ICNP)*, Nov. 2016, pp. 1–10.

[24] A. M. López, G. Fernández, and F. Burillo, "Mobile computing with near field communication (NFC) smart objects applied to archaeological research," in *Proc. 12th Int. Conf. Intell. Environ. (IE)*, Sep. 2016, pp. 88–94.

[25] Y. Liu, J. Yang, and M. Liu, "Recognition of QR code with mobile phones," in *Proc. IEEE Chin. Control Decision Conf.*, New York, NY, USA, Jul. 2008, pp. 203–206.

[26] B. G. A. Kumar, K. C. Bhagyalakshmi, K. Lavanya, and K. H. Gowranga, "A Bluetooth low energy based beacon system for smart short range surveillance," in *Proc. IEEE Int. Conf. Recent Trends Electron., Inf. Commun. Technol. (RTEICT)*, May 2016, pp. 1181–1184.
[27] S. Alletto *et al.*, "An indoor location-aware system for an IoT-based smart museum," *IEEE Internet Things J.*, vol. 3, no. 2, pp. 244–253, Apr. 2016.
[28] K. Sornalatha and V. R. Kavitha, "IoT based smart museum using Bluetooth low energy," in *Proc. 3rd Int. Conf. Adv. Elect., Electron., Inf., Commun. Bio-Inform. (AEEICB)*, Feb. 2017, pp. 520–523.
[29] N. Golmie, R. E. Van Dyck, A. Soltanian, A. Tonnerre, and O. Rébala, "Interference evaluation of Bluetooth and IEEE 802.11b systems," *Wireless Netw.*, vol. 9, no. 3, pp. 201–211, 2003.
[30] P. Bihler, P. Imhoff, and A. B. Cremers, "SmartGuide—A smartphone museum guide with ultrasound control," *Procedia Comput. Sci.*, vol. 5, pp. 586–592, Aug. 2011. [Online]. Available: http://www.sciencedirect.com/science/article/pii/S1877050911004017
[31] J. Jeon, G. Chae, and W. S. Yeo, "Developing a location-aware mobile guide system for GLAMs based on TAPIR sound tag: A case study of the lee ungno museum," in *Human-Computer Interaction. Applications and Services*. Cham, Switzerland: Springer, 2014, pp. 425–433. [Online]. Available: https://doi.org/10.1007/978-3-319-07227-2_40
[32] (2016). *Raspberry PI 3 Model B*. [Online]. Available: https://www.raspberrypi.org/products/raspberry-pi-3-model-b/
[33] E. Trevisani and A. Vitaletti, "Cell-ID location technique, limits and benefits: An experimental study," in *Proc. 6th IEEE Workshop Mobile Comput. Syst. Appl. (WMCSA)*, Dec. 2004, pp. 51–60.
[34] F. J. Álvarez, T. Aguilera, J. Morera, and J. A. Moreno, "GUIMUS: A smartguide based on an acoustic FSK protocol, " in *Proc. Int. Conf. Indoor Positioning Indoor Navigat. (IPIN)*, Oct. 2016, pp. 1–4.
[35] Kingstate Electronics Corp. (2016). *KSSG1708 High-Frequency Transducer*. [Online]. Available: http://www.kingstate.com.tw/index.php/en/component/k2/item/66
[36] (2016). *STM32L4 Series of Ultra-Low-Power MCUs*. [Online]. Available: http://www.st.com/en/microcontrollers/stm32l4-series.html?querycriteria=productId=SS1580
[37] N. Levanon and E. Mozeson, *Radar Signals*. New York, NY, USA: Wiley, 2004.
[38] *Acoustics—Attenuation of Sound During Propagation Outdoors—Part 1: Calculation of the Absorption of Sound by the Atmosphere*, document ISO 9613-1:1993, International Organization for Standarization, 1993.
[39] D. T. Blackstock, *Fundamentals of Physical Acoustics*. New York, NY, USA: Wiley, 2000.
[40] (2016). *LG X Screen, LGK500N*. [Online]. Available: http://www.lg.com/uk/mobile-phones/lg-K500N
[41] (2016). *JTransforms Libraries*. [Online]. Available: https://sites.google.com/site/piotrwendykier/software/jtransforms
[42] (2016). *Android Studio SDK*. [Online]. Available: https://developer.android.com/studio/index.html
[43] O. B. Matar, J. P. Remenieras, A. Roncin, and F. Patat, "Non contact measurement of vibration using airborne ultrasound," in *Proc. IEEE Ultrason. Symp.*, vol. 1. Nov. 1996, pp. 697–700.

Fernando J. Álvarez (M'07–SM'17) received the B.S. and M.S. degrees in physics from the University of Seville, Seville, Spain, the M.S. degree in electronic engineering from the University of Extremadura, Badajoz, Spain, the M.S. degree in signal theory and communications from the University of Vigo, Vigo, Spain, and the Ph.D. degree in electronics from the University of Alcalá, Alcalá de Henares, Spain.

In 2008, he was a Post-Doctoral José Castillejo Fellow with the Intelligent Sensors Laboratory, Yale University, New Haven, CT, USA. He is currently an Associate Professor of digital electronics with the Department of Electrical Engineering, Electronics and Automation, University of Extremadura, where he is also the Head of the Sensory Systems Group. His current research interests include local positioning systems, acoustic signal processing, and embedded computing.

Teodoro Aguilera received the B.S. and M.S. degrees in physics and the Ph.D. degree in electronics from the University of Extremadura, Badajoz, Spain, in 2011 and 2016, respectively.

He was an Assistant Professor of automation for three years with the Department of Electrical Engineering, Electronics and Automation, University of Extremadura, where he is currently a Research Member of the Sensory Systems Group and involved in the design of acoustic local positioning systems based on mobile devices.

José A. Paredes received the Degree in physics and the M.S. degree in engineering and architecture research from the University of Extremadura, Badajoz, Spain, in 2010 and 2012, respectively.

He is involved mainly in digital signal processing. He is currently a Laboratory Assistant with the Sensory Systems Group, University of Extremadura, where he is involved in the design of local positioning systems based on different technologies.

José A. Moreno received the Degree in computer engineering from the University of Deusto, Bilbao, Spain, in 1993.

He is currently an Associate Professor of digital systems and microprocessors with the Department of Electrical Engineering, Electronics and Automatics, University of Extremadura, Badajoz, Spain. His current research interests include reconfigurable computing, embedded computing, and digital signal processing systems.